Earth and Planetary Science Letters 317-318 (2012) 218–230

Contents lists available at SciVerse ScienceDirect

Earth and Planetary Science Letters

journal homepage: www.elsevier.com/locate/epsl

A 750-kyr detrital-layer stratigraphy for the North Atlantic (IODP Sites U1302–U1303, Orphan Knoll, Labrador Sea)

J.E.T. Channell [a,*], D.A. Hodell [b], O. Romero [c], C. Hillaire-Marcel [d], A. de Vernal [d], J.S. Stoner [e], A. Mazaud [f], U. Röhl [g]

[a] Dept. of Geological Sciences, University of Florida, Gainesville, FL 32611, USA
[b] Godwin Laboratory for Palaeoclimate Research, Dept. of Earth Sciences, University of Cambridge, Cambridge, UK
[c] Inst of Earth Sciences of Andalucia, Universidad de Granada, Granada, Spain
[d] GEOTOP, Université du Québec a Montreal, Montreal, QC, Canada
[e] College of Oceanic and Atmospheric Sciences, Oregon State University, Corvallis, OR, USA
[f] Laboratoire des Sciences du Climat et de l'Environnement, CEA-CNRS, Gif-sur-Yvette, France
[g] MARUM — Center for Marine Environmental Sciences, University of Bremen, Leobener Strasse, Bremen 28359, Germany

ARTICLE INFO

Article history:
Received 21 July 2011
Received in revised form 17 November 2011
Accepted 21 November 2011
Available online xxxx

Editor: P. DeMenocal

Keywords:
Orphan Knoll
North Atlantic
Heinrich layers
Relative paleointensity
XRF core scanning
Chinese speleothems

ABSTRACT

Integrated Ocean Drilling Program (IODP) Sites U1302–U1303, drilled on the SE flank of Orphan Knoll (Labrador Sea), preserve a record of detrital layers and other proxies of hydrographic change that extend the record of ice-sheet/ocean interactions through most of the Brunhes Chron. The age model is built by tandem matching of relative paleointensity (RPI) and oxygen isotope data ($\delta^{18}O$) from *Neogloboquadrina pachyderma* (sin.) to reference records, indicating a mean Brunhes sedimentation rate of 14 cm/kyr. Sedimentation back to marine isotope stage (MIS) 18 is characterized by detrital layers that are detected by higher than background gamma-ray attenuation (GRA) density, peaks in X-ray fluorescence (XRF) indicators for detrital carbonate (Ca/Sr) and detrital silicate (Si/Sr), and an ice-rafted debris (IRD) proxy (wt.% > 106 μm). The age model enables correlation of Site U1302/03 to IODP Site U1308 in the heart of the central Atlantic IRD belt where an age model and a similar set of detrital-layer proxies have already been derived. Ages of Heinrich (H) layers H1, H2, H4, H5 and H6 are within ~2 kyr at the two sites (H0, H3 and H5a are not observed at Site U1308), and agree with previous work at Orphan Knoll within ~3 kyr. At Site U1308, Brunhes detrital layers are restricted to peak glacials and glacial terminations back to marine isotope stage (MIS) 16 and have near-synchronous analogs at Site U1302/03. Detrital layers at Site U1302/03 are distributed throughout the record in both glacial and most interglacial stages. We distinguish Heinrich-like layers associated with IRD from detrital layers marked by multiple detrital-layer proxies (including Ca/Sr) but usually not associated with IRD, that may be attributed to lofted sediment derived from drainage and debris-flow events funneled down the nearby Northwest Atlantic Mid-Ocean Channel (NAMOC). The prominent detrital layers at Sites U1302/03 and U1308 can be correlated to millennial scale features in the Chinese speleothem (monsoon) record over the last 400 kyr, implying a link between monsoon precipitation and Laurentide Ice Sheet (LIS) instability. The detrital-layer stratigraphy at Site U1302/03 provides a long record of LIS dynamics against which other terrestrial and marine records can be compared.

1. Introduction

Ice sheet–ocean interactions are both forced by, and influence, climate. During the last glacial period, Laurentide Ice Sheet (LIS) instability is recorded by detrital carbonate layers, known as Heinrich events, in sediment cores from the North Atlantic (Broecker et al., 1992; Heinrich, 1988). These events had far-reaching impacts on climate through fresh-water forcing and its impact on Atlantic Meridional Overturning Circulation (AMOC) (e.g. Clark et al., 2002). Few long records of ice rafted debris (IRD) exist for periods beyond the last glacial interval, with notable exceptions including ODP Site 980 (McManus et al., 1999) and IODP Site U1308 (Hodell et al., 2008). Here we document a North Atlantic detrital-layer stratigraphy, for the last 750 kyrs, that represents a history of iceberg discharges from the LIS, set within a robust chronological framework.

The correlation of Heinrich-like detrital layers across the North Atlantic is important for understanding their origin and significance, but presents a stratigraphic challenge owing to their millennial-scale recurrence time, particularly at Orphan Knoll close to conduits for detritus from the Laurentide and Greenland ice sheets, where the frequency of detrital input is greater than at more distal sites. Heinrich's (1988) paper documented detrital layers during the last glacial interval in the

* Corresponding author at: Dept. Geological Sciences, POB 112120, University of Florida, Gainesville, FL 32611, USA. Tel.: +1 352 392 3658; fax: +1 352 392 9294.
E-mail address: jetc@ufl.edu (J.E.T. Channell).

0012-821X/$ – see front matter © 2011 Elsevier B.V. All rights reserved.
doi:10.1016/j.epsl.2011.11.029

eastern North Atlantic, based on high lithic fragment percentages (close to 100%) in the 180–3000 μm grain size fraction. The presence of detrital carbonate, derived from the lower Paleozoic basins of northern Canada, was found to be a diagnostic feature of these detrital layers that are largely comprised of IRD supposedly deposited by armadas of icebergs emanating from the LIS during the last glacial interval (Bond et al., 1999; Broecker et al., 1992; Hemming, 2004). Heinrich layers are typically identified based on a combination of high IRD content, presence of detrital carbonate, minima in planktic foraminiferal accumulation rates, and predominance of *Neogloboquadrina pachyderma* (sin.) in the foraminiferal assemblage (e.g. Hillaire-Marcel et al., 1994; Hiscott et al., 2001; Rashid et al., 2003; Rasmussen et al., 2003; van Kreveld et al., 1996), augmented by high magnetic susceptibility and a coarsening in magnetic grain size (e.g. Robinson et al., 1995; Stoner et al., 1996, 2000). Studies of Heinrich events have been largely focused on the last glacial cycle (encompassing H0-H6) in the central Atlantic (e.g. Bond and Lotti, 1995; Bond et al., 1993, 1999; Grousset et al., 1993; van Kreveld et al., 1996), the Labrador Sea (e.g. Andrews and Tedesco, 1992; Hillaire-Marcel et al., 1994; Hiscott et al., 2001; Rashid et al., 2003; Stoner et al., 2000), the Irminger Basin off east Greenland (e.g. Elliot et al., 1998), and the NW European margin (Peck et al., 2007; Scourse et al., 2000, 2009; Walden et al., 2006). Sources of IRD in these regions may include not only Laurentia and Greenland, but also Europe and Iceland. Owing to the existence of the Greenland ice cores as stratigraphic templates and the availability of radiocarbon dating for the last ~50 kyr, a relatively detailed understanding of ice sheet ocean interactions has been developed over the last glacial–interglacial cycle.

The objective of the present paper is fourfold: (1) Establish an age model for IODP Sites U1302–U1303 (hereafter referred to as Site U1302/03), located close to Orphan Knoll, Labrador Sea (Fig. 1), based on oxygen isotope and paleomagnetic data; (2) Develop a Labrador Sea detrital layer stratigraphy for the site that extends through the Brunhes Chronozone; (3) Use the age models to correlate the detrital layer stratigraphy from Site U1302/03 to Site U1308, located 1720 km east of Site 1302/03 (Fig. 1) in the central part of the North Atlantic IRD belt (Ruddiman, 1977). (4) Identify the presence of Heinrich events prior to the last glacial cycle that may have had global climate significance, and are therefore likely to be manifested in other climate records.

2. Site descriptions

2.1. IODP Site U1308 (Eastern IRD belt)

Integrated Ocean Drilling Program (IODP) Site U1308 constitutes a reoccupation of Deep Sea Drilling Project (DSDP) Site 609, a site that has been pivotal in the study of Heinrich layers and encompassing

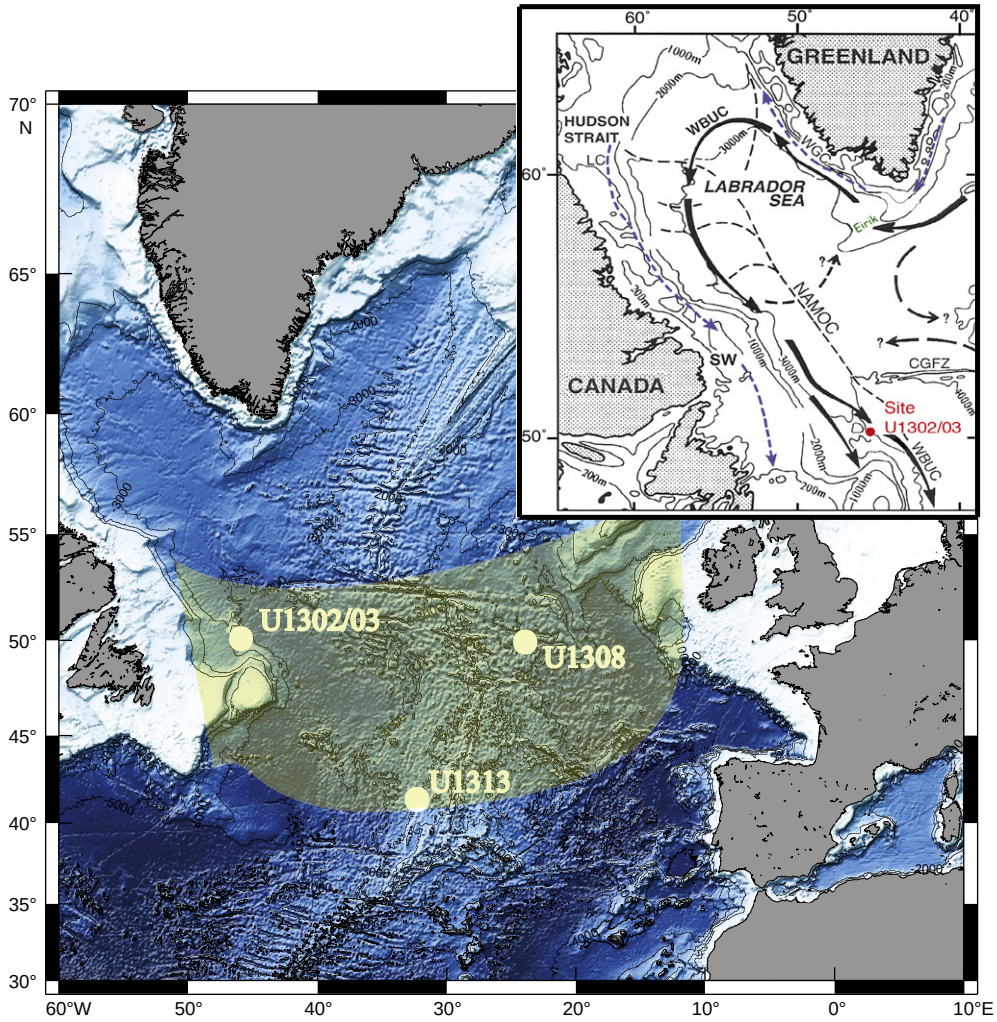

Fig. 1. Location for IODP Sites U1302/03, U1308 and U1313. Yellow shading indicates the approximate extent of the Ruddiman (1977) ice rafted debris (IRD) belt. Inset: Location for Site U1302/03 showing deep (black arrows) and surface (blue arrows) current trajectories. Abbreviations: WGC, West Greenland Current; LC, Labrador Current; WBUC, western boundary under current; NAMOC, Northwest Atlantic mid-ocean channel; CGFZ, Charlie Gibbs fracture zone; Eirik, Eirik Drift (after Hillaire-Marcel and Bilodeau, 2000). (For interpretation of the references to color in this figure legend, the reader is referred to the web version of this article.)

Bond cycles, and of their correlation to Greenland ice-core records during the last glacial–interglacial cycle (Bond and Lotti, 1995; Bond et al., 1993, 1999). At Site U1308, detrital layers were detected using gamma-ray attenuation porosity evaluator (GRAPE) density measurements, bulk carbonate $\delta^{18}O$, and Ca/Sr and Si/Sr ratios derived from XRF core scanning (Hodell et al., 2008). The Ca/Sr ratio distinguishes detrital carbonate from biogenic carbonate due to the high proportion of Sr in biogenic carbonate relative to chemically formed carbonate, and is therefore suitable for the detection of layers dominated by detrital calcite. Similarly, bulk carbonate $\delta^{18}O$ may reflect the proportion of biogenic to detrital carbonate, and resembles the lithic-to-foraminifera ratio at DSDP Site 609 (Hodell and Curtis, 2008). The Si/Sr ratio can be used to detect detrital layers rich in silicate grains, although peaks in this ratio often coincide with Ca/Sr minima indicating that low flux of (detrital and biogenic) carbonate affects the Si/Sr ratio. At Site U1308, "Hudson-Strait" derived Heinrich-like layers, characterized by detrital carbonate, appear in marine isotope stage (MIS) 2 and 3, MIS 8, MIS 10, MIS 12 and MIS 16, but not in MIS 6 and 14 or glacial periods beyond MIS 16 (Hodell et al., 2008). Alkenone-based sea-surface temperature data from the central Atlantic (IODP Site U1313, Fig. 1) suggest that the first appearance of Heinrich-like layers in MIS 16 (Stein et al., 2009) is not primarily related to low sea-surface temperature (SST) or iceberg survivability (Naafs et al., 2011), but instead represents a fundamental change in ice-sheet dynamics (Hodell et al., 2008). Ji et al. (2009) used Fourier Transform Infrared Spectrophotometry (FTIR) to determine percent dolomite, as a proxy for detrital carbonate, over the last ~480 kyr at Site U1308. Dolomite peaks are associated with H1–H6, the MIS 5a/5b boundary (H7), MIS 5/6 boundary (H11), MIS 7/8 boundary, MIS 9/10 boundary and MIS 11/12 boundary, with higher than background dolomite in glacial intervals MIS 6, MIS 8, MIS 10 and MIS 12, and at the MIS 7a/7b boundary.

2.2. IODP Site U1302/03 (Orphan Knoll)

IODP Site U1302 (50° 10′N, 45° 38.3′W, water depth: 3560 m) and Site U1303 (50° 12.4′N, 45°41.2′W, water depth: 3520 m) were occupied during IODP Expedition 303 to the North Atlantic (Fig. 1). The two sites are located off the Newfoundland continental margin just to the south of a seamount known as Orphan Knoll (minimum water depth: 1800 m). The sites are 5.7 km (3 nmi) apart, lie on the SE flank of the Knoll and are positioned on a rise between two canyons that help to funnel turbidites and debris flows away from the site (Channell et al, 2006). Debris flows shed from fault scarps, apparently during MIS 5 and MIS 7, appear in seismic reflection records from this region (Toews and Piper, 2002) and the locations of Sites U1302 and U1303 were chosen to avoid them. Drilling at Site U1302, however, encountered a debris flow in the 107–132 meters composite depth (mcd) interval, at the base of the Brunhes Chronozone, and the same debris flow was found (close to the same depth) at Site U1303. The two sites were found to be remarkably similar and can be correlated without difficulty using shipboard multisensor track (MST) data (Expedition 303 Scientists, 2006). A short segment from one core of Site U1303 (Core U1303B-1H), together with the record from Site U1302, provides a continuous composite stratigraphic sequence to ~104 mcd. Two holes were drilled at Site U1303. Although five holes were drilled at Site U1302, two of them (Holes U1302D and U1302E) comprised only two cores, drilled specifically to recover the sediment–water interface. Lithologies are clay and silty clay with nannofossil ooze down to 104 mcd, overlying debris flows that comprise intraclasts in a matrix of sand, silt and clay (Expedition 303 Scientists, 2006).

Conventional piston cores collected near Orphan Knoll by R/V *Hudson* (e.g., Core HU91-045-94P) and *Marion Dufresne* (e.g., Cores MD95-2024 and MD99-2237) have previously recovered numerous detrital layers deposited during the last glacial–interglacial cycle that have been tied to Heinrich Layer stratigraphies for the last 110 kyr using radiocarbon ages, planktic $\delta^{18}O$ stratigraphy (Hillaire-Marcel et al., 1994; Stoner et al., 1998) and ice core chronologies (Stoner et al., 2000) following the correlation of detrital layers to cold stadials in the Greenland Summit ice cores (Bond et al., 1993). Other cores from the vicinity of Orphan Knoll preserve a lithologic record associated with LIS instabilities, namely cores to the west (Cores HU92-045-11P, MD95-2025 and MD99-2233) (Hiscott et al., 2001), and to the south (EW9302-1/2JPC) (Rasmussen et al., 2003), as well as from the crest of Orphan Knoll itself (EW9303-31) (Bond and Lotti, 1995). The Orphan Basin cores to the west of the Knoll are notable as they provide the only records from the region, up to now, extending beyond the last climate cycle, back to 340 ka in the case of Core MD95-2025 (Hiscott et al., 2001). Rapidly deposited detrital layers in the Orphan Knoll region have been detected by weight % of the >125 μm or 150 μm fraction, weight % carbonate and planktic $\delta^{18}O$ (Bond and Lotti, 1995; Hillaire-Marcel et al., 1994; Rasmussen et al., 2003), a "Heinrich variable" comprising counts of rock and silicate grains divided by the count of rock and silicate grains plus foraminifera (Hiscott et al., 2001), and magnetic grain-size and concentration parameters (Stoner et al., 1995, 1996, 1998, 2000). There is undoubtedly an IRD component in these detrital layers, but there may also be a component deposited from suspension derived from turbiditic flow in the nearby Northwest Atlantic Mid-Ocean Channel (NAMOC), a deep-sea channel that lies along the axis of the Labrador Sea (Fig. 1) and is a conduit for turbiditic sediment transport into the North Atlantic related to LIS instability (Hesse et al., 1997, 2004; Hillaire-Marcel et al., 1994; Stoner et al., 1996). Cores HU91-045-94P, MD95-2024 and MD99-2237 were all collected at about the same location as Site U1303. Interestingly, the two *Marion Dufresne* (MD) cores extend into MIS 6 at ~25 meters below seafloor (mbsf) indicating an apparent mean sedimentation rate of ~17 cm/kyr; however, the HU (R/V *Hudson*) core reaches into MIS 5c (~100 kyr) level at ~11 mbsf, implying a mean sedimentation rate of ~11 cm/kyr. At Site U1302/03, the top of MIS 6 is at 15.6 mbsf, indicating a mean sedimentation rate back to MIS 6 of 12 cm/kyr, implying that the MD cores are affected by severe core stretching. Detrital layers correlate to H0, H1, H2, H3, H4 and H5 were identified in Core HU91-045-94P, as well as three low-detrital-carbonate (LDC) layers between H1 and H2 (Stoner et al., 1996, 1998). Rashid et al. (2003) introduced the label H5a to refer to the detrital-carbonate event (DC6) at ~52–53 ka (Stoner et al., 1998), between H5 and H6. Apart from detrital layers in the last glacial interval, Hiscott et al. (2001) recognized detrital layers within MIS 5c (H8), and at Terminations II and III in Core MD95-2025.

3. Methods

The $\delta^{18}O$ record at Site U1302/03 is based on the previously published record of Hillaire-Marcel et al. (2011) that was derived from the planktic foraminifer *Neogloboquadrina pachyderma* (sin.), due to the paucity of benthic foraminifera at this site. Sediment samples were first sieved at 106 μm, then ultrasonically cleaned and finally sieved at 150 μm. An average of 12 specimens (about 80 μg) picked from the 150–250 μm size fraction were reacted at 90 °C with >100% orthophosphoric acid, using a Multicarb™ preparation device online with a dual inlet IsoPrime™ mass spectrometer (see details in Hillaire-Marcel et al., 2011). Samples were analyzed at 5-cm intervals down-core, and results are reported as δ-values against VPDB (see Coplen, 1996). The weight percentage (wt.%) of the >106 μm grain size fraction is used as an IRD proxy. The biogenic content of the >106 μm fraction, comprising a small number of foraminifera, is negligible compared to the detrital component, and, in the context of the Labrador Sea, the >106 μm wt.% fraction is considered a satisfactory IRD proxy.

For Quaternary deep-sea sediments, oxygen isotope ($\delta^{18}O$) stratigraphies provide the traditional means of temporal correlation. Age models are often developed through correlations to calibrated reference records (e.g. Lisiecki and Raymo, 2005), usually through ties at glacial–interglacial transitions (Terminations). The position of Terminations can be significantly offset from the global continental ice volume signal, even for benthic $\delta^{18}O$, by local variations in water temperature, salinity

and chemistry (e.g. Lisiecki and Raymo, 2009; Skinner and Shackleton, 2005). In addition, at high latitudes, planktic isotopic records may be strongly perturbed by ice-surges, meltwater events and/or the production of isotopically light brines due to sea-ice growth, particularly near major conduits for meltwater such as the Labrador Sea (e.g. Hillaire-Marcel, 2011). Here we utilize the tandem correlation of (planktic) $\delta^{18}O$ and relative (geomagnetic) paleointensity (RPI) in an effort to improve on the resolution of stratigraphic correlation afforded by $\delta^{18}O$ alone.

The natural remanent magnetization (NRM) of u-channel samples (2x2x150 cm^3 "continuous" samples collected from 150-cm long core sections) was measured at 1-cm intervals, with a 10-cm leader and trailer at the top and base of each sample, using a 2G Enterprises pass-through magnetometer at the University of Florida designed for u-channel measurements (e.g. Weeks et al., 1993). After initial NRM measurement, stepwise AF demagnetization was carried out in 5 mT increments in the 20–60 mT interval and 10 mT increments in the 60–100 mT interval. The intensity of a detrital remanent magnetization (DRM) depends on the intensity of the geomagnetic field, and the concentration and alignment efficiency of remanence-carrying grains. In favorable circumstances, the relative strength of the magnetizing field can be determined by using the intensity of different types of laboratory-induced magnetizations, anhysteretic remanence and isothermal remanence (ARM and IRM), to normalize the NRM intensity for changes in concentration of remanence-carrying grains. The resulting normalized remanence can be a proxy for RPI variations (Banerjee and Mellema, 1974; King et al., 1983; Levi and Banerjee, 1976; Tauxe, 1993). Our procedure for determining RPI proxies is to calculate three slopes (see Channell et al., 2002, 2008): slopes of NRM-lost versus (1) ARM-lost, (2) ARMAQ (ARM acquisition) and (3) IRM-lost, determined over specific demagnetization (acquisition) intervals. These three slopes are equivalent to calculating the NRM/ARM, NRM/ARMAQ and NRM/IRM ratios, and are accompanied by linear correlation coefficients (r) that yield the linearity (precision) of each slope, calculated at 1-cm intervals down-core. As part of the process of determining RPI proxies, stepwise demagnetization of NRM was used to determine the base of Brunhes Chronozone, which occurs close to the base of the recovered sedimentary section.

At Site U1302/03, we use a similar battery of detrital layer proxies used by Hodell et al. (2008) at Site U1308, including XRF proxies for detrital layers (Ca/Sr and Si/Sr), and gamma ray attenuation porosity (GRA density). For procedures for XRF core scanning at Site U1302/03, see Hodell et al. (2008). The Ca/Sr and Si/Sr ratios, measured at 1-cm intervals along the composite section, are sensitive to the presence of detrital carbonate and silicate, respectively. For procedures for shipboard measurement of density using the gamma ray attenuation porosity evaluator (GRAPE), see Channell et al (2006).

4. Paleomagnetism and paleointensity

Shipboard paleomagnetic measurements at Site U1302/03 comprised pass-through measurements of archive halves at 5 cm intervals using demagnetizing fields not exceeding 20 mT (Expedition 303 Scientists, 2006). The maximum peak field was restricted so that core sections would not be compromised for shore-based magnetic investigations described here. The archive halves of the composite section at Site U1302/03 were sampled using u-channels at the IODP core repository in Bremen. In addition, several u-channels were collected below the base of the composite section (below 104 mcd), in order to search for the Matuyama–Brunhes boundary. The shipboard measurements did not succeed in recording the base of the Brunhes Chronozone, due to the presence of debris flows at the base of the section (Expedition 303 Scientists, 2006).

Component NRM declinations and inclinations from u-channel samples were computed for the 20–80 mT demagnetization interval (Fig. 2) by standard least-squares methods (Kirschvink, 1980) without anchoring to the origin of the orthogonal projections, using UPmag software (Xuan and Channell, 2009). The maximum angular deviation (MAD) values indicate variations in the quality of the component directions down section with values below 5°, indicating well-defined magnetization directions (Fig. 2) carried by a low-coercivity mineral, known from earlier studies in the region to be magnetite (e.g. Stoner et al., 1995). MAD values exceed 10° in some intervals, particularly close to the base of the section and in the vicinity of apparent magnetic excursions (the evidence for magnetic excursions at this site will be the subject of a subsequent paper). MAD values would be lowered by choosing individualized demagnetization ranges for individual measurements or individual measurement intervals, however, the calculation for a global (20–80 mT) demagnetization range, and accompanying MAD values, allow a more straightforward assessment of the quality of the directional record (Fig. 2). Declinations were adjusted for vertical-axis core rotation by uniform rotation of each core so that the mean declination for each core is oriented North or South for positive and negative inclination intervals, respectively (Fig. 2). The component magnetization directions indicate that the section above the debris flows is within the Brunhes Chronozone, with the Matuyama Chronozone apparently recorded by sediments immediately below the upper debris flows (Fig. 2). U-channels were not collected from the debris flows themselves but from intercalated undeformed silts and clays free of pebble-sized debris.

In Fig. 2, we plot slopes of NRM/ARM, NRM/ARMAQ and NRM/IRM, and associated linear correlation coefficients (r) for the 20–60 mT peak field demagnetization/acquisition range. The slopes constitute three alternative relative paleointensity (RPI) proxies and the three proxies are fairly consistent giving us confidence in the RPI record (Fig. 2), and the linear correlation coefficients (r) are close to unity indicating that the slopes are reasonably well defined within this (20–60 mT) demagnetization/acquisition interval. The NRM/IRM record is associated with many of the r-values below 0.98, probably due to the greater affect of coarse magnetite grains (that do not contribute significantly to NRM) on IRM relative to ARM. For the age model, we utilize only the NRM/ARM proxy, which closely matches the NRM/ARMAQ proxy.

5. Age model

The age model for the Site U1302/03 was constructed by tandem fitting of $\delta^{18}O$ and RPI to reference curves, the reference curves being the PISO-1500 RPI stack (Channell et al., 2009) and the LR04 benthic $\delta^{18}O$ stack (Lisiecki and Raymo, 2005). The tandem correlations were performed using the "Match" protocol (Lisiecki and Lisiecki, 2002) that is capable of optimizing correlations for two pairs of ostensibly independent but global signals (see Channell et al., 2009). The advantage of Match over visual matching is that Match correlations are repeatable, which is unlikely to be the case for visual correlations, particularly visual correlations involving independent pairs of signals. The Match procedure involves the choice of penalty functions that minimize the likelihood of sedimentation rate changes within and between time/depth series.

Our procedure for generating the Site U1302/03 age model is as follows. (1) Tandem *visual* correlation of the $\delta^{18}O$ record to LR04 and the RPI record to the PISO-1500 stack yielding 30 initial (not fixed) tie-points. (2) Application of Match to the $\delta^{18}O$ and RPI records using the LR04 and PISO-1500 stacks as calibrated reference templates. (3) Comparison of correlation coefficients for the visual and Match correlations. Both $\delta^{18}O$ and RPI (Pearson) correlation coefficients indicate that the Match correlation (0.77 for $\delta^{18}O$ and 0.65 for RPI) is an improvement over the visual correlation (0.68 for $\delta^{18}O$ and 0.52 for RPI).

In Fig. 3, the Site U1302/03 planktic $\delta^{18}O$ record, on the age model described above, is compared with the LR04 benthic $\delta^{18}O$ stack of Lisiecki and Raymo (2005). The accompanying Site U1302/03 RPI record is shown together with the PISO-1500 reference stack (Channell et al., 2009). The isotopic record from *N. pachyderma* (sin.) is marked by light $\delta^{18}O$ excursions, particularly at Terminations and also during

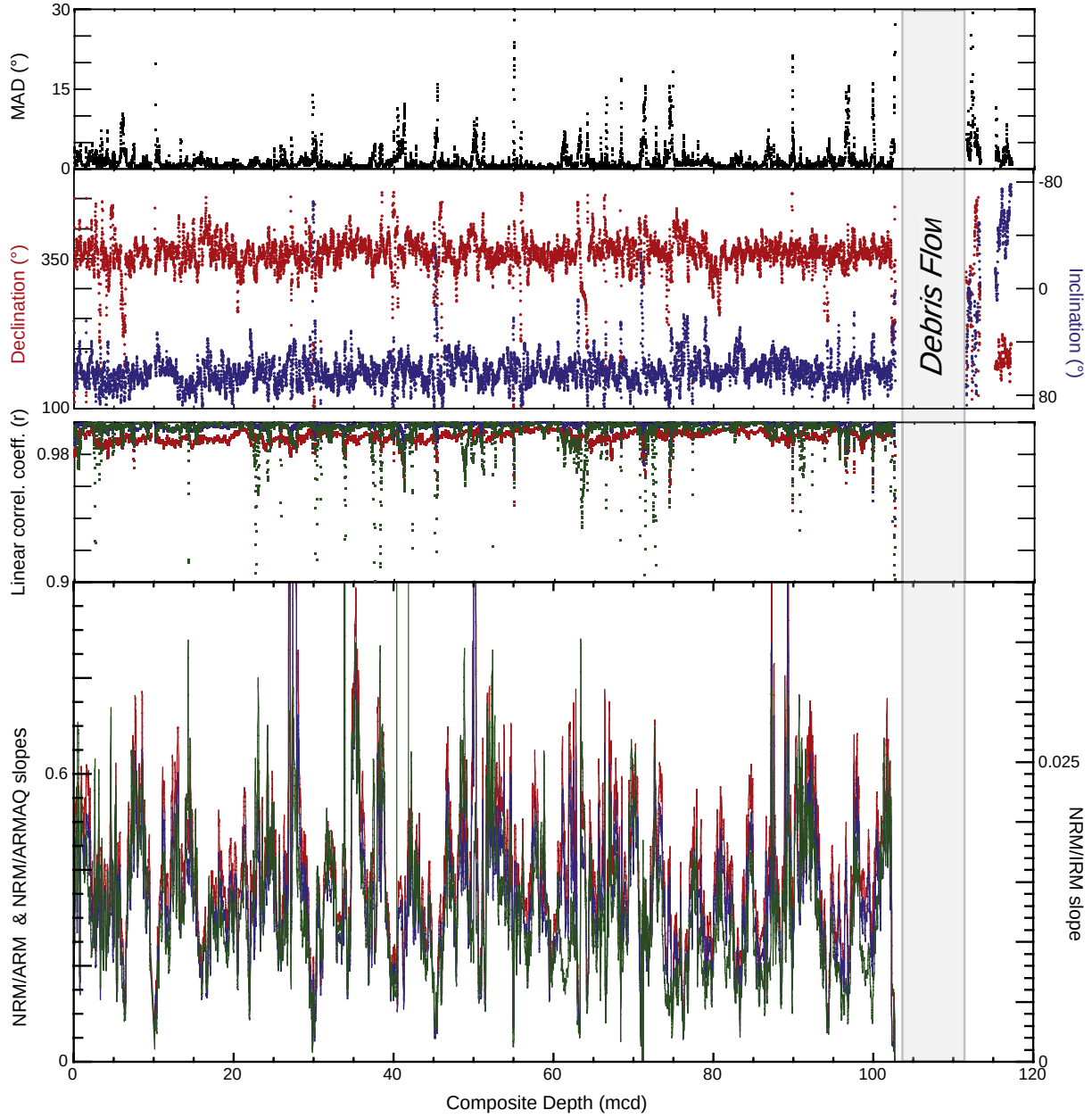

Fig. 2. IODP Site U1302/03 paleomagnetic data from u-channel samples: component inclination, declination, maximum angular deviation (MAD) values computed for the 20–80 mT demagnetization interval, and relative paleointensity (RPI) proxies: slopes of NRM/ARM (red), NRM/ARMAQ (blue) and NRM/IRM (green) for the 20–60 mT demagnetization and acquisition interval, with corresponding linear correlation coefficients (r). (For interpretation of the references to color in this figure legend, the reader is referred to the web version of this article.)

Heinrich-like detrital events. These isotopic excursions relate to meltwater pulses and to sea-ice formation accompanied by isotopically-light brine rejection (see Hillaire-Marcel and de Vernal, 2008), which complicate the use of the $\delta^{18}O$ record as a stratigraphic tool.

The resulting Site U1302/03 sedimentation rates are plotted in Fig. 4, together with sedimentation rates from IODP Site U1308 (Hodell et al., 2008), and the sedimentation rates for Site U1302/03 based on the $\delta^{18}O$ data alone (Hillaire-Marcel et al., 2011). The sedimentation rates derived here differ from those implied from $\delta^{18}O$ data alone, and the offset of the $\delta^{18}O$ record placed on the two age models is particularly apparent in MIS 5, MIS 8–9 and MIS 15–18 (Fig. 4). Note that sedimentation rates are rather uniform in the MIS 9–12 interval although this is an interval where the chronological utility of both the $\delta^{18}O$ record and the RPI record is perturbed by unusual/barren sediments, particularly at the MIS 9/10 boundary (Termination IV).

6. Detrital layer stratigraphy

The age model described above is applied to proxies for detrital layers at Site U1302/03 in Figs. 5–7. These figures include the $\delta^{18}O$ and RPI data on which the age model is based, and Site U1308 data from Hodell et al. (2008). The detrital layer proxies comprise XRF scanning ratios sensitive to layers rich in (inorganic) carbonate and silicate-rich detritus (Ca/Sr and Si/Sr), bulk carbonate $\delta^{18}O$ that is sensitive to the relative proportion of biogenic and detrital carbonate (Hodell and Curtis, 2008), and GRAPE density. In Figs. 5–7, these parameters are plotted to indicate detrital layers as peaks trending up-page. Detrital layers

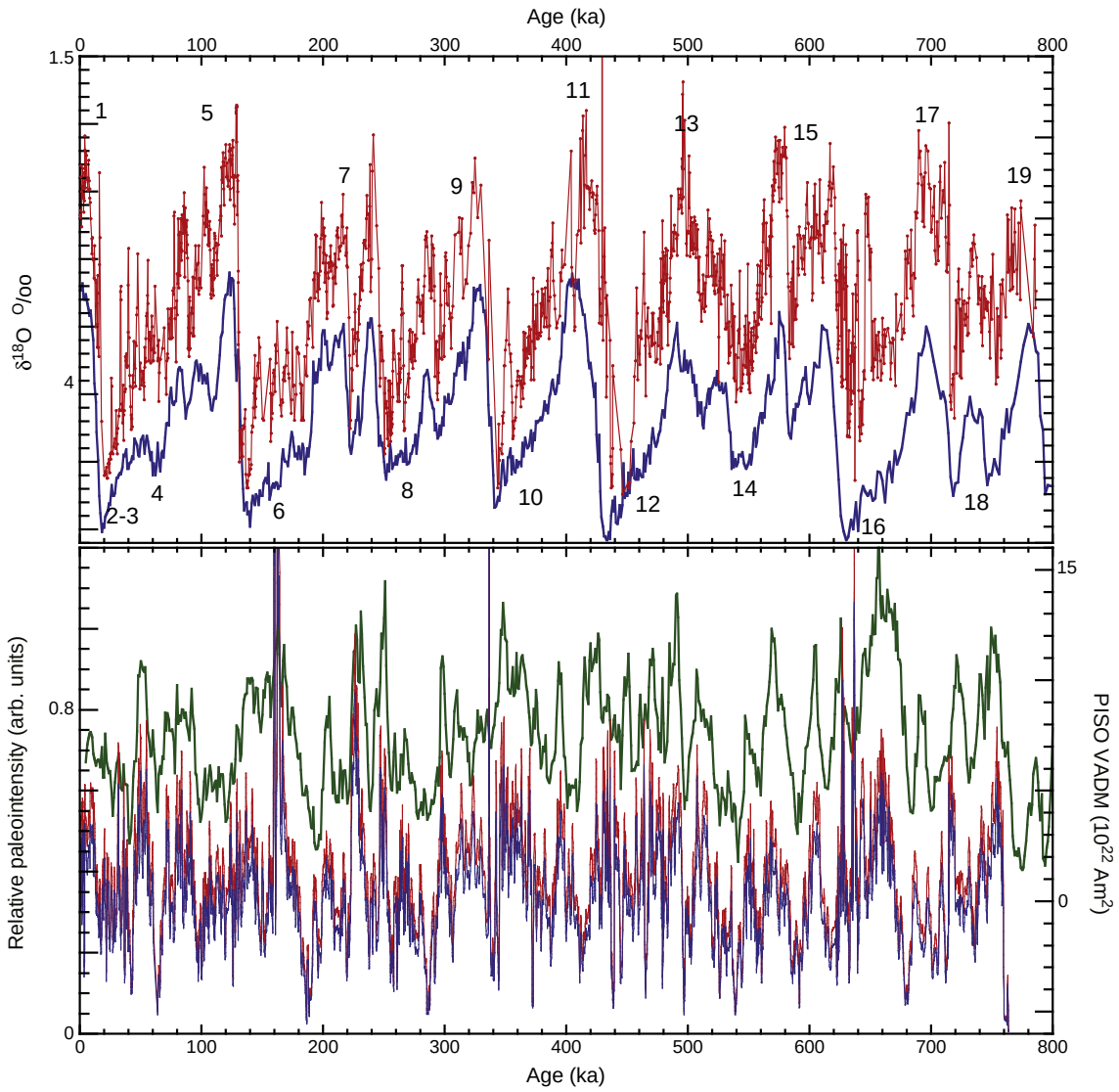

Fig. 3. Top: Planktic oxygen isotope record from Site U1302/03 (red) with marine oxygen isotope stages marked, compared with the LR04 benthic oxygen isotope stack (blue, Lisiecki and Raymo, 2005). Base: Relative paleointensity proxies (NRM/ARM, red, and NRM/ARMAQ, blue), compared with the PISO-1500 RPI stack, green (Channell et al., 2009). (For interpretation of the references to color in this figure legend, the reader is referred to the web version of this article.)

are marked by higher than background XRF ratios, higher GRAPE density, and lower than background bulk-carbonate $\delta^{18}O$. The prominent detrital layers at Site U1302/03 beyond and including H11 (~128 ka) are numbered from youngest to oldest with a prefix corresponding to the marine isotope stage in which they are found (Figs. 5–7). Detrital layers associated with Terminations (terminal ice rafting events or TIREs in the terminology of Venz et al., 1999) are labeled with prefixes appropriate for the older (glacial) stage.

Peaks in Si/Sr often correspond to minima in Ca/Sr due to high silicate (clay) concentration corresponding to low carbonate; however, in some instances at Site U1308, Ca/Sr and Si/Sr peaks coincide, indicating multiple detrital sources rather than lows in Sr due to lows in biogenic carbonate (e.g. Site U1308 detrital layer equivalents to H5 in Fig. 5 and Event 8.3 in Fig. 6). Ca/Sr peaks at both sites are associated with highs in GRAPE density, and lows in bulk carbonate $\delta^{18}O$.

6.1. Glacial stages

As discussed above, the detrital layer stratigraphy for the last glacial interval at Orphan Knoll is well known from studies in the 1990s (e.g. Hillaire-Marcel et al., 1994; Veiga-Pires and Hillaire-Marcel, 1998) and detrital layers from this location have been correlated to cold stadials in Greenland ice cores thereby generating rather precise age models derived from ice-core chronologies (Stoner et al., 2000). Our age model at Site U1302/03 is not over-defined in this interval with few changes in sedimentation rate (Fig. 4), and is based on the automated match of planktic $\delta^{18}O$ and RPI to reference templates. The resulting ages of H1–H6 at Site U1302/03 (Table 1) are within a few kyr of those at Site U1308 (Hodell et al., 2008) and consistent with earlier results from Orphan Knoll (Stoner et al., 1998, 2000). Note that the Site U1302/03 age model takes no account of the duration of Heinrich events, estimated to be ~1000 yr (Hemming, 2004; Veiga-Pires and Hillaire-Marcel, 1998), and their enhanced sedimentation rate relative to background.

At Site U1302/03, H0–H5a are marked by the XRF Ca/Sr ratio, GRAPE density, and planktic and bulk $\delta^{18}O$ (Fig. 5). H6 differs from the younger Heinrich events. In core section 1302C-1H-4, part of the composite section, the H6 interval is manifest by a 20 cm thick silty sand (at 99–119 cm depth in the section), overlying a 20 cm thick cream-colored clay layer (95% clay) devoid of foraminifera with

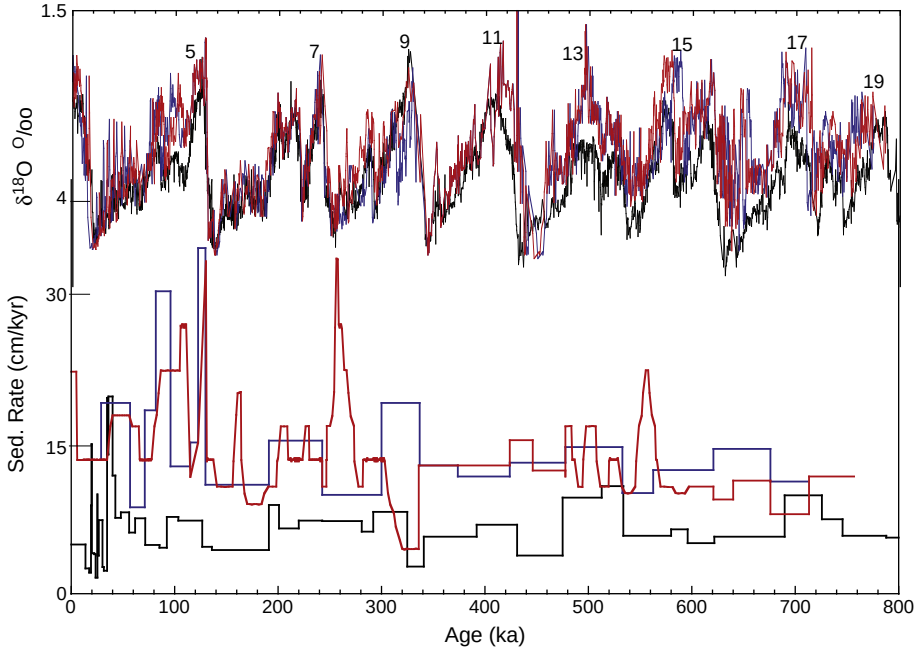

Fig. 4. Top: Oxygen isotope ($\delta^{18}O$) records for Site U1302/03 on the age model used here (red), and the age model of Hillaire-Marcel et al. (2011) (blue), and the Site U1308 $\delta^{18}O$ record on its own age model (black, Hodell et al., 2008). Marine isotope stages are labeled. Base: Sedimentation rates for Site U1302/03 on the age model used here (red) and on the age model of Hillaire-Marcel et al. (2011) (blue), and Site U1308 sedimentation rates (black, Hodell et al., 2008). (For interpretation of the references to color in this figure legend, the reader is referred to the web version of this article.)

exceptionally low Ca/Sr, and GRAPE density. Immediately below this cream-colored layer is an interval rich in IRD, marked by the abundance of the >106 μm grain-size fraction (Fig. 5).

At Site U1308, H1, H2, H4 and H5 are manifested by Ca/Sr, GRAPE density, and planktic and bulk $\delta^{18}O$ (Fig. 5). Heinrich layers H3, H5a and H6 are not marked by these parameters at Site U1308 although H3 and H6, at Site U1308, correspond to broad peaks in Si/Sr and lows in bulk carbonate $\delta^{18}O$ (Fig. 5).

During MIS 6, five detrital layers are recognized at Site U1302/03. H11 (Event 6.1) is marked by the IRD (>106 μm) proxy, Ca/Sr, and GRAPE density (Fig. 5). At Site U1308, H11 coincides with Termination II and is manifest as a Si/Sr peak and low in bulk carbonate $\delta^{18}O$ (Fig. 5). At Site U1302/03, within late MIS 6, prominent Ca/Sr and Si/Sr features (labeled 6.2 and 6.3 in Fig. 5) are accompanied by GRAPE density, and >106 μm anomalies. Smaller peaks in these same parameters mark events 6.4 and 6.5 during early MIS 6 (Fig. 6).

During MIS 8, four detrital layers are identified at Site 1302/03. Three of these (8.1, 8.2 and 8.3) are also marked by Ca/Sr peaks at Site 1308 with Event 8.4 possibly marked by an increase in Si/Sr and decrease in bulk carbonate $\delta^{18}O$. Event 8.1 is the TIRE that marks the transition from MIS 8 to interglacial MIS 7 (i.e., Termination III).

During MIS 10, three detrital layers are identified at Site U1302/03. At both Site U1302/03 and Site U1308, the MIS 9/10 boundary (Termination IV) is poorly defined by the $\delta^{18}O$ record due to clay-rich sediments devoid of foraminifera in the boundary interval (Fig. 6). As a result of this, and perturbation of the Site U1302/03 RPI record in the IRD-rich interval (340–350 ka) at the Termination, the age model in the MIS 9/10 boundary interval is poorly constrained. This contributes to the mismatch of detrital events between the two sites close to the MIS 9/10 boundary. We speculate that the prominent detrital layer that appears at the onset of MIS 9 at Site U1308 is equivalent to the TIRE (labeled 10.1) at Site U1302/03 (Fig. 6). Events 10.2 and 10.3 appear to be marked by Si/Sr peaks at Site U1308.

At Site U1302/3, MIS 12 exhibits seven detrital layers with distinct (>106 μm) IRD signals. Event 12.1 represents the TIRE associated with Termination V and occurs at both Sites U1302/03 and U1308. The number and pacing of the Heinrich events during MIS 12 (12.1 through 12.7) were apparently similar to that in the last glacial period (Table 1). Some of the events are expressed as peaks in Si/Sr at Site U1308.

MIS 14, which was a short weak glacial period, contains perhaps a single, poorly defined, detrital layer at both sites (Fig. 7). MIS 16 contains four detrital layers at Site U1302/03. Two of these (16.1 and 16.2) are also manifest by Ca/Sr peaks at Site U1308. Event 16.1 is the TIRE associated with Termination VI. At Site U1302/03, Event 16.1 is a complex event in which the IRD pulse coincides with a Si/Sr peak which immediately predates the Ca/Sr peak, with a similar juxtaposition of the Ca/Sr and Si/Sr peaks at Site U1308 (Fig. 7). MIS 18 appears to exhibit four events at Site U1302/03 with a TIRE (Event 18.1) that shows a similar structure to Event 16.1, although all MIS 18 events have muted IRD signatures relative to younger Heinrich-like detrital layers.

6.2. Interglacial stages

At Site U1302/03, the detrital events are not limited to glacial intervals but also occur during interglacial stages. Unlike detrital layers deposited during glacial intervals, however, the interglacial detrital layers are not always associated with an increase in the >106 μm fraction. At Site U1302/03, numerous peaks in Ca/Sr occur throughout MIS 5 (Fig. 5). The Ca/Sr ratio in MIS 5 is mimicked by GRAPE density and the >106 μm IRD proxy. The >106 μm parameter implies that IRD is an intermittent constituent of deposition within MIS 5 and other interglacials. Indeed, shipboard core descriptions noted the presence of pebble (>2 mm) dropstones throughout the section at Site U1302/03, except in peak interglacials such as MIS 5e and MIS 11 (see Fig. F10 in Expedition 303 Scientists, 2006). Two Ca/Sr peaks close to the MIS 5a/5b boundary (labeled H7/H7a in Fig. 5) are also manifest in the GRAPE density record. At the MIS 5c/5d boundary, and apparently within MIS 5c, Ca/Sr and GRAPE density features are accompanied by elevations in the >106 μm IRD proxy. In contrast, the detrital layer proxies in MIS 5 at Site U1308 are generally

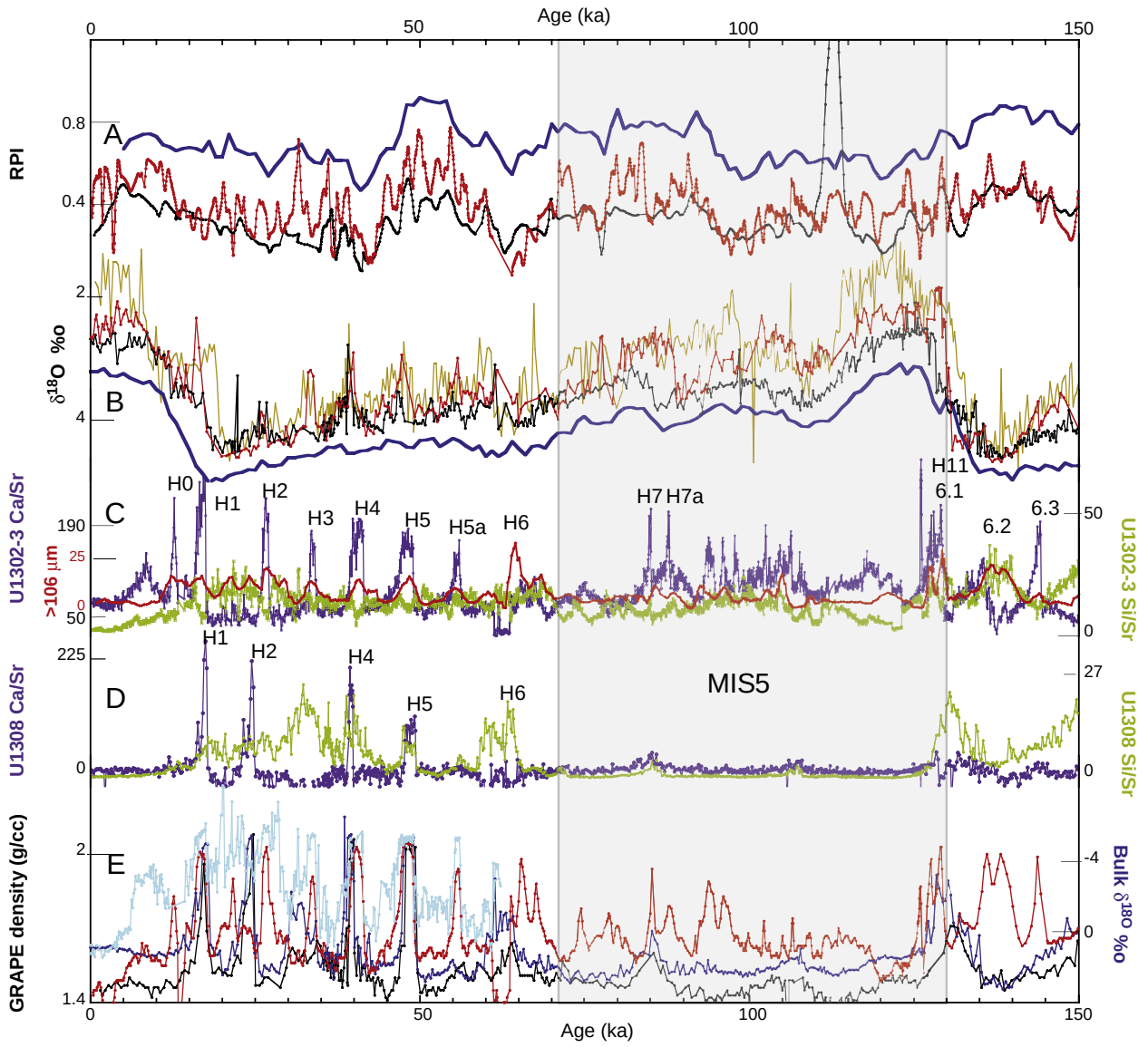

Fig. 5. Interval 0–150 ka: (A) Relative paleointensity proxies for Site U1302/03 (red) and Site U1308 (black) compared with RPI reference stack (PISO-1500) of Channell et al. (2009) (blue). (B) Site U1302/03 planktic $\delta^{18}O$ (red), Site U1308 benthic and planktic $\delta^{18}O$ (black and brown) with LR04 (blue). (C) Site U1302/03 XRF scanning Ca/Sr (blue) and Si/Sr (green), wt.% >106 μm grain size fraction (red). (D) Site U1308 XRF scanning Ca/Sr (blue) and Si/Sr (green). (E) Site U1302/03 GRAPE density (red) and Site U1308 GRAPE density (black), with bulk carbonate $\delta^{18}O$ for Site U1302/03 for 0–62 ka (light blue) and at Site U1308 (dark blue). All detrital-layer proxies plotted to indicate detrital carbonate (Ca/Sr) and detrital silicates (Si/Sr) increasing up, GRAPE density increasing upward. Detrital events (not necessarily Heinrich-like) are labeled sequentially for each marine isotope stage beyond MIS 5. (For interpretation of the references to color in this figure legend, the reader is referred to the web version of this article.)

flat and featureless (Fig. 5). Ji et al. (2009) observed a dolomite peak at the MIS 5a/5b boundary at Site U1308 which they labeled H7.

During MIS 7, two detrital layers are recognized at Site 1302/03 but they are not associated with peaks in the >106 μm IRD proxy. Similarly, two detrital layers are recorded in MIS 9, six in MIS 13, and two events in MIS 15. In all cases, the peaks in Ca/Sr and density, that define these interglacial detrital layers, do not coincide with peaks in the (>106 μm) IRD proxy. On the other hand, some of them (e.g. Event 13.3) appear to have IRD peaks associated with their bases and tops (Fig. 7). One prominent Si/Sr event in MIS 17 at Site U1308, coincident with a low in Ca/Sr, is not apparently synchronous with a prominent MIS 17 Ca/Sr event (17.1) at Sites U1302–U1303 (Fig. 7).

7. Comparison of Sites U1302/03 and U1308

The age model allows a reasonable match of the detrital layer stratigraphy at Site U1302/03 to that of Site U1308 back to H6 (~60 ka), and with less clarity back to MIS 18 (Fig. 8). Numerous detrital events are recorded in the last glacial interval at Site U1302/03, four of which are clearly synchronous with detrital events at Site U1308: H1, H2, H4 and H5 (Figs. 5 and 8). H3 is marked at Site U1302/03 by Ca/Sr, GRAPE density, and a prominent planktic and bulk $\delta^{18}O$ minimum. H3 is not manifest by a Ca/Sr peak at Site U1308 but as a broad Si/Sr peak (Fig. 5). At Site U1302/03, the H6 interval comprises a ~20 cm thick silty sand overlying a (~25 cm thick) cream-colored clay that is devoid of carbonate that is, in turn, underlain by a (50 cm-thick) IRD rich interval (Fig. 5). The cream-colored clay layer can be interpreted as deposited from suspension as a result of a massive debris flow or drainage event (possibly funneled down the nearby NAMOC) that immediately postdates an IRD event. Note that H6 does not have the LIS detrital carbonate signature of younger Heinrich events. In some cases at Site U1302/03, planktic $\delta^{18}O$ minima lag detrital layer proxies such as Ca/Sr, GRAPE density and bulk $\delta^{18}O$ (e.g. H4 and H5, Fig. 5) and the IRD (>106 μm) peaks are sometimes located at bases and

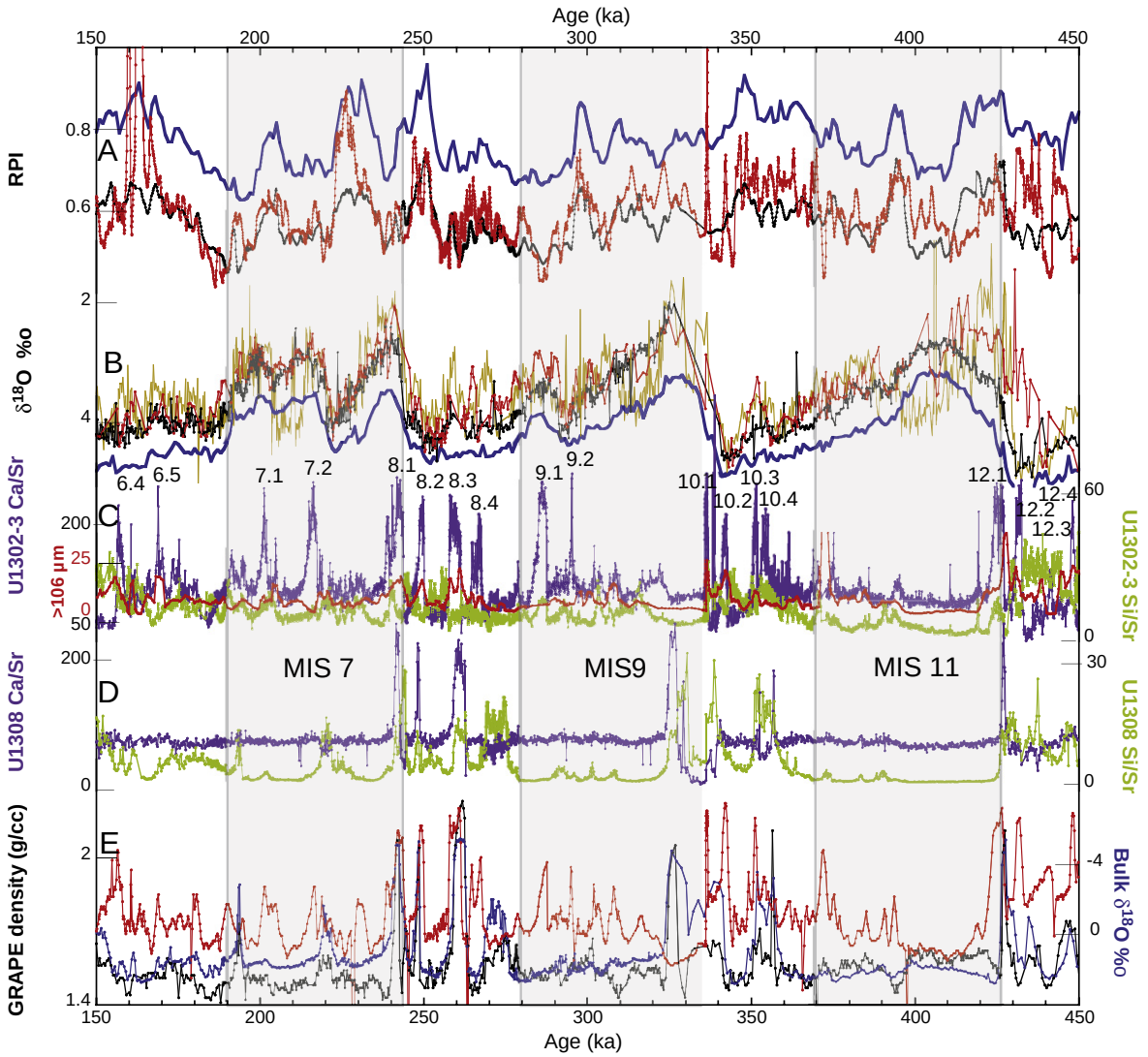

Fig. 6. Interval 150–450 ka: Relative paleointensity and oxygen isotope data, and proxies for detrital layers at Site U1302/03 and Site U1308. Key (A–E) as for Fig. 5.

tops of detrital layers (Figs. 6 and 7). For H0 and H1 in Core HU91-045-94P (Clarke et al., 1999; Veiga-Pires and Hillaire-Marcel, 1998), IRD deposition apparently preceeded NAMOC-related deposition possibly analogous to the 8.2 ka drainage episode of Lake Agassiz (Hillaire-Marcel et al., 2007; Kleiven et al., 2008). Increasing buoyancy in meltwater-derived turbidity currents, as the sediment load is deposited, can lead to rising plumes containing fine-grained detritus (Sparks et al., 1993) that may account for the widespread deposition of NAMOC-related suspended sediment, associated with Heinrich events, at Orphan Knoll and throughout the Labrador Sea (see Hesse et al., 2004).

Many detrital events recorded at Site U1302/03 are apparently not recorded at Site U1308, either due to iceberg survival and transport trajectory, or because NAMOC-related depositional processes that affect Site U1302/3 in the deep Labrador Sea are too local to be recorded at distal Site U1308. On the other hand, all Ca/Sr events at Site U1308 appear to have analogues at Site U1302/03 albeit with offsets for H2 and Event 10.1 attributable to age model discrepancies (Fig. 8), and some Si/Sr events at Site U1308 do not have analogues at Site U1302/03 implying non-LIS detrital sources (Figs. 5–8).

Unlike Site U1308, detrital layers at Site U1302/03 are apparently not restricted to Terminations and peak glacials but occur in all glacial stages and all interglacial stages other than MIS 11. Interglacial detrital layers at Site U1302/03 are indicated by some detrital layer proxies (Ca/Sr, GRAPE density), although they are not usually associated with an increase in the >106 µm defined IRD fraction. We speculate that they are not necessarily directly related to LIS surges, but rather to NAMOC debris flows or glacial-lake drainage events as a result of important changes in base level and/or hydrological budget.

Si/Sr ratios are markedly elevated within glacial stages at Site U1308 and Site U1302/03, attributable to low biogenic carbonate content. The timing of Si/Sr events does not usually coincide with Ca/Sr events at either site, although there are a few examples at Site U1308 where this is the case (e.g. Site U1308 equivalents to Site U1302/03 Event 8.3 and Event 16.1). The presence of foraminifera in these intervals implies that reduction of biogenic carbonate (Sr) does not, in itself, explain the coincidence of Ca/Sr and Si/Sr peaks.

All Heinrich-like detrital layers that are correlated between the two sites, as well as the labeled Heinrich-like layers that are observed at Site U1302/03 only, occur where benthic δ^{18}O values exceed 3.5‰ during glacial periods (Fig. 8). At ODP Site 980, McManus et al. (1999) observed that this same threshold represented an increase in iceberg discharge and sea-surface temperature variability in the North Atlantic. The increased occurrence of Heinrich-like detrital layers implies a

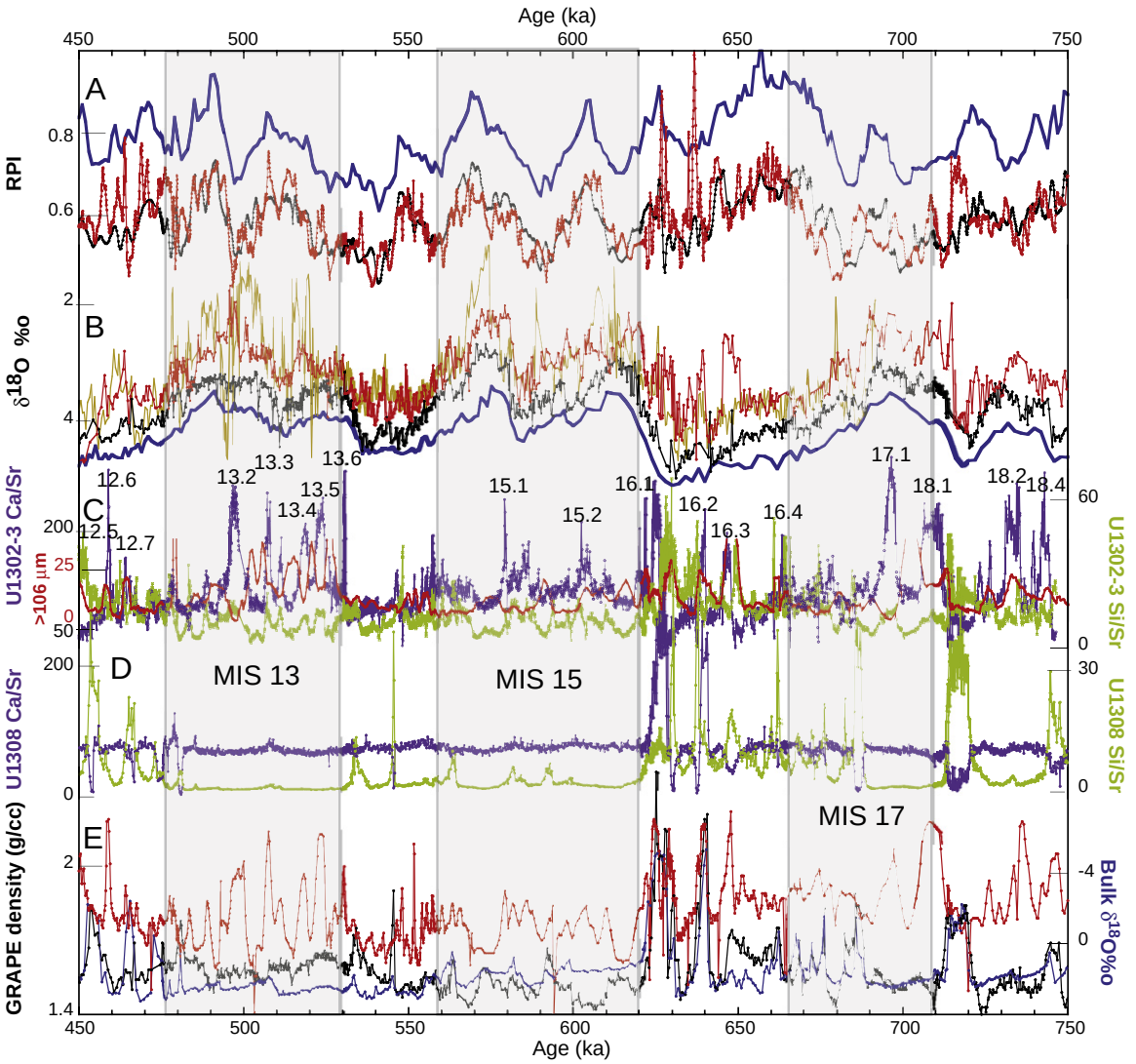

Fig. 7. Interval 450–750 ka: Relative paleointensity and oxygen isotope data, and proxies for detrital layers at Site U1302/03 and Site U1308. Key (A–E) as for Fig. 5.

physical threshold in continental ice volume above which the likelihood of triggering ice-sheet surges is enhanced. We also note that the Heinrich-like detrital layers in peak glacial stages (MIS 6 to MIS 18) are bunched into groups with a persistent ~6–10 kyr recurrence time (Table 1), reminiscent of MIS 3, and possibly related to cyclic changes in basal temperature of the LIS (see MacAyeal, 1993).

Table 1
Comparison of ages of Heinrich events H0–H6 from various authors, and other Heinrich-like events on the Site U1302/03 age model, with the ages of plausibly correlative features in the Chinese speleothem record (Fig. 9) in parentheses. Ages of Heinrich-like detrital events (ka) over last ~750 kyr.

	H0	H1	H2	H3	H4	H5	H5a	H6		
Core HU91-045-94P Orphan Knoll (Stoner et al., 1998)	12	16.5	23	29	35.5	48	59	63		
Core MD95-2024 Orphan Knoll (Stoner et al., 2000)		15.5	24	30	39.5	46	52.5	59.5		
Hemming (2004) review article		16.8	24	31	38	45		60		
Site U1302/03 (this paper)	**12.7 (12.3)**	**17.1 (15.8)**	**26.7 (24.3)**	**33.7 (30.5)**	**40.7 (38.8)**	**48.0 (48.0)**	**55.7 (55.5)**	**63.5 (60.1)**		
Site U1308 (Hodell et al., 2008)		17.5	24.5		39.4	48.6		63.5		
Site U1302/03										
Labels for Heinrich-like events	H6.1 (H11)	H6.2	H6.3	H6.4	H6.5	H7.1	H7.2	H8.1	H8.2	H8.3
Ages (ka) for Heinrich-like events	128.5 (130.7)	135.5 (138.6)	144.3 (149.5)	157.0 (161.8)	168.9 (170.2)	201.2 (199.7)	216.2 (217.6)	242.4 (243.5)	249.4 (249.8)	259
Labels for Heinrich-like events	H8.4	H10.1	H10.2	H10.3	H10.4	H12.1	H12.2	H12.3	H12.4	H12.5
Ages (ka) Heinrich-like events	266	336.8 (338.5)	342	352	355	424	430	438	444	458
Labels for Heinrich-like events	H12.6	H12.7	H16.1	H16.2	H16.3	H16.4	H18.1	H18.2	H18.3	H18.4
Ages (ka) Heinrich-like events	465	478	625	640	647	663	697	709	733	743

Ages in parentheses are ages of presumed correlative features in the Chinese speleothem record (see Fig. 9)

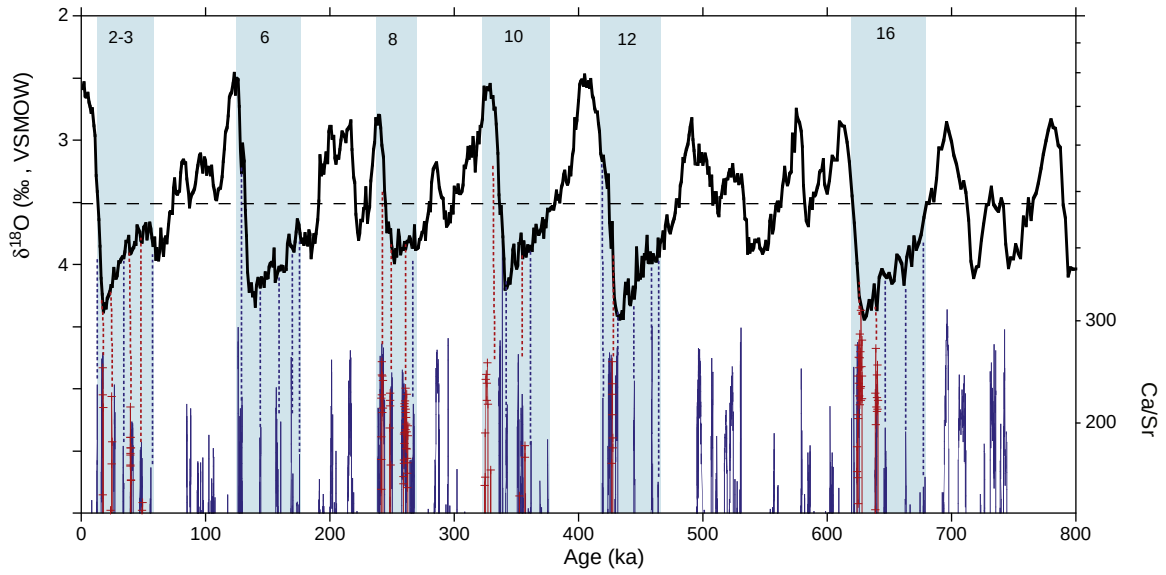

Fig. 8. XRF Ca/Sr for Site U1302/03 (blue) and Site U1308 (red) compared with the LR04 benthic oxygen isotope stack (black, Lisiecki and Raymo, 2005). Dashed horizontal line indicates 3.5‰ threshold value for $\delta^{18}O$ (see text). Prominent glacial intervals are marked by blue shading. (For interpretation of the references to color in this figure legend, the reader is referred to the web version of this article.)

8. Comparison with Chinese speleothem $\delta^{18}O$

The $\delta^{18}O$ of Chinese speleothem calcite records the summer/winter (monsoon) precipitation ratio and is closely tied to Northern Hemisphere summer insolation, punctuated by numerous millennial-scale events that resemble the Greenland ice-core $\delta^{18}O$ implying a link between the intensity of the East Asian Monsoon and Greenland air-temperatures (e.g. Wang et al., 2001). In view of this apparent link, the composite Chinese speleothem $\delta^{18}O$ record from Hulu Cave (Wang et al., 2001), Dongge Cave (Dykoski et al., 2005) and Sanbao Cave (Cheng et al., 2009; Wang et al., 2008) with its orbital-scale variations removed (Barker et al., 2011) is compared with the detrital layer (Ca/Sr) record from Sites U1302/03 and U1308 (Fig. 9). Such a comparison permits an evaluation of our timescale relative to a radiometrically-dated (U–Th) speleothem record. Making the assumption that features in these two records are indeed synchronous, we provide absolute age estimates for some of the North Atlantic detrital carbonate events (Table 1).

The correlations imply that Site U1302/03 and Site U1308 age models, based partly or entirely on correlation to the benthic LR04 oxygen isotope stack, often lag the U–Th-dated speleothem record (Fig. 9, Table 1). Note, however, that the lag for Site U1308 at Termination IV (~340 ka, Fig. 9b) is an artifact of a poorly constrained Site U1308 age model in this interval, due to barren sediments across the Termination. From analysis of the Chinese speleothem record, Cheng et al. (2009) did not observe a clear lag between insolation rise and ice sheet response over the last few Terminations. The lag between LR04-assisted age models, at Site U1302/03 and Site U1308, and the speleothem chronology may be related to time constants (lags) used in ice-volume models that calibrate LR04 and other marine oxygen isotope records. On the other hand, the apparent lag of detrital Heinrich-like layers (Fig. 9) could also be attributed to asynchronous Terminations (e.g. Skinner and Shackleton, 2005), or slight shifts in timing due to how the speleothem $\delta^{18}O$ data were filtered to remove orbital variations (Barker et al., 2011).

9. Paleoclimate implications

The freshwater forcing associated with the larger Heinrich events, especially those recorded at both Sites U1302/03 and U1308, are likely to have disrupted Atlantic Meridional Overturning Circulation (AMOC) and have manifestations not only in Chinese speleothem records but also in other regional or global climate records. Each of the glacial terminations is associated with terminal ice-rafting events (TIREs), similar to H1 for the last deglaciation (Hodell et al., 2008). These dynamic events probably triggered and/or hastened the demise of the ice sheets during deglaciation through strong feedback processes (Alley and Clark, 1999; Hughes, 2011), and may have played an important role in glacial terminations (Cheng et al., 2009; Denton et al., 2010). Changes in ice-sheet stability, related to basal boundary conditions, likely played an important role in determining the style and timing of glacial terminations (Hughes, 2011; Marshall and Clark, 2002).

10. Conclusions

Detrital layer stratigraphy at IODP Site 1302/03 (Orphan Knoll, Labrador Sea) can be correlated to detrital layer stratigraphy at IODP Site U1308 (central Atlantic), over the last 750 kyr, using age models based of oxygen isotope and relative paleointensity (RPI) data. Whereas detrital layers are restricted to peak glacial intervals back to MIS 16 at Site U1308, detrital layers at Site U1302/03 are found in both glacial and interglacial intervals, although interglacial detrital layers are not always associated with IRD and may include a component deposited from suspension derived from NAMOC-related turbidity currents and flood events. The detrital layers at both IODP sites can be plausibly correlated to millennial-scale features in the Chinese speleothem record, implying a link between monsoon precipitation and LIS instability.

Acknowledgments

We thank V. Lukies and H. Pfletschinger for assistance with XRF core scanning, K. Huang for assistance in the UF paleomagnetic laboratory, D. Lee for help with age models, and A. Wülbers and W. Hale for their help at the IODP Bremen Core Repository. This research was supported by US National Science Foundation Grants OCE-0850413 and OCE-1014506 to J.C., UK National Environmental Research Council Award NE/H009930/1 to D.A.H., and grants from the Natural Sciences and Engineering Research Council (NSERC) of Canada, the *Fonds Québecois sur la Recherche et les Technologies* (FQRNT) and the Canadian Foundation for Climate and Atmospheric Sciences (CFCAS) to C.H.-M. and A.d.V., and the Deutsche Forschungsgemeinschaft to U.R.

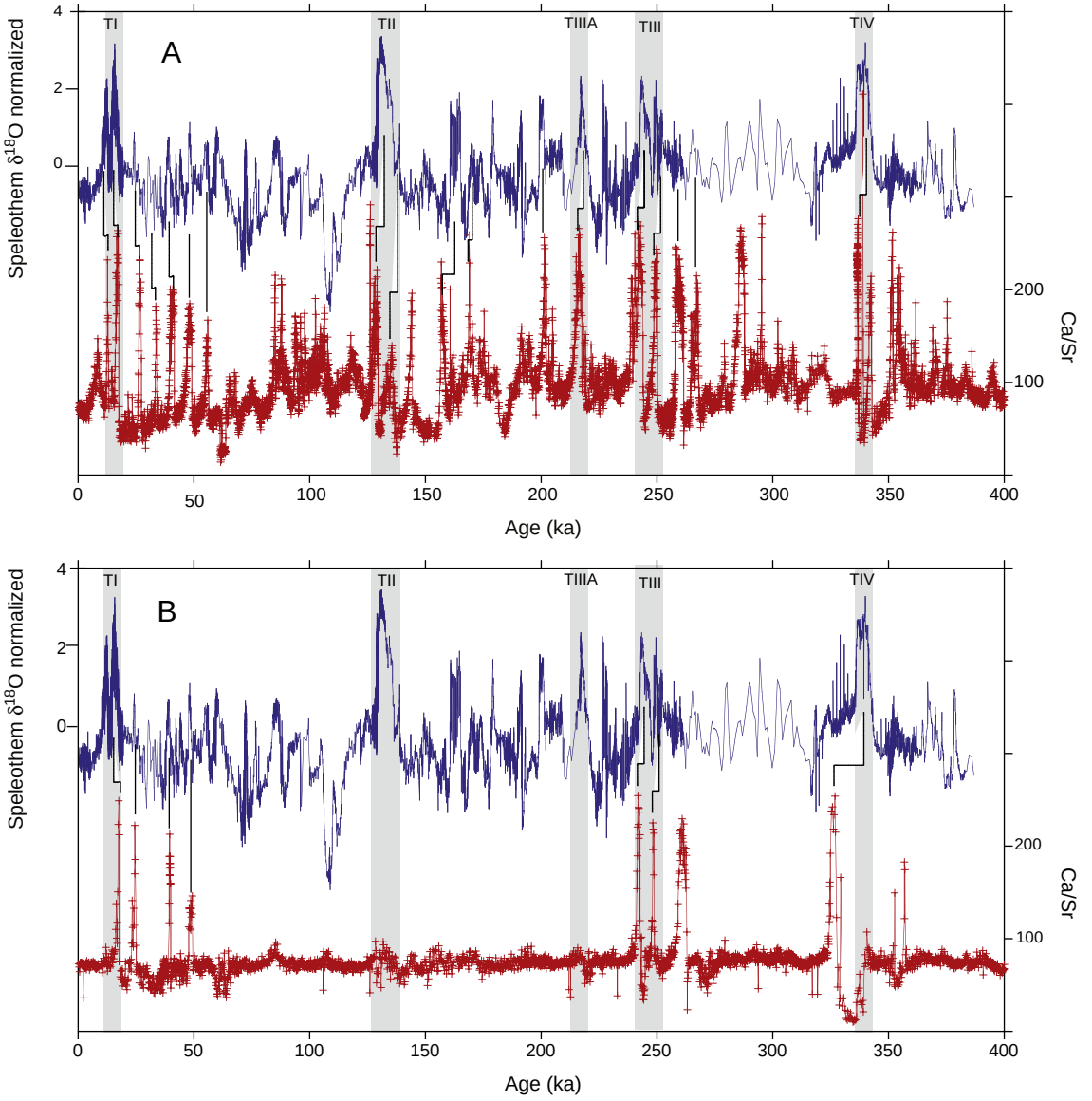

Fig. 9. The Chinese speleothem record (Cheng et al., 2009; Dykoski et al., 2005; Wang et al., 2001, 2008) with the orbital-scale variations removed (Barker et al., 2011) in blue, compared with the XRF Ca/Sr records (red) from (a) Site U1302/03 and (b) Site U1308. Heinrich-like detrital layers can be tentatively correlated to the speleothem timescale (see Table 1). (For interpretation of the references to color in this figure legend, the reader is referred to the web version of this article.)

References

Alley, R.B., Clark, P.U., 1999. The deglaciation of the northern hemisphere: a global perspective. Ann. Rev. Earth Planet. Sci. 27, 149–182.

Andrews, J.T., Tedesco, K., 1992. Detrital carbonate-rich sediments, northwestern Labrador Sea: implications for ice-sheet dynamics and iceberg rafting(Heinrich) events in the North Atlantic. Geology 20, 1087–1090.

Banerjee, S.K., Mellema, J.P., 1974. A new method for the determination of paleointensity from the ARM properties of rocks. Earth Planet Sci. Lett. 23 (1974), 177–184.

Barker, S., Knorr, G., Lawrence Edwards, R., Parrenin, F., Putnam, A.E., Skinner, L.C., Wolff, E., Ziegler, M., 2011. 800,000 years of abrupt climate variability. Science 334, 347–351.

Bond, G., Lotti, R., 1995. Iceberg discharges into the North Atlantic on millennial time scales during the last glaciation. Science 267, 1005–1010.

Bond, G., Broecker, W., Johnsen, S., McManus, J., Laberyie, L., Jouzel, J., Bonani, G., 1993. Correlations between climate records from North Atlantic sediments and Greenland ice. Nature 365, 143–147.

Bond, G., Showers, W., Elliot, M., Evans, M., Lotti, R., Hajdas, I., Bonani, G., Johnson, S., 1999. The North Atlantic's 1–2 kyr climate rhythm: relation to Heinrich events, Dansgaard/Oeschger cycles and the little ice age. In: Webb, et al. (Ed.), Mechanisms of Millennial-Scale Global Climate Change: AGU Geophysical Monograph Series, 112, pp. 35–58.

Broecker, W.S., Bond, G., Klas, M., Clark, F., McManus, J., 1992. Origin of the northern Atlantic's Heinrich events. Climate Dyn. 6, 265–273.

Channell, J.E.T., Mazaud, A., Sullivan, P., Turner, S., Raymo, M.E., 2002. Geomagnetic excursions and paleointensities in the 0.9–2.15 Ma interval of the Matuyama Chron at ODP Site 983 and 984 (Iceland Basin). J. Geophys. Res. 107 (B6). doi:10.1029/2001JB000491.

Channell, J.E.T., T. Kanamatsu, T. Sato, R. Stein, C.A. Alvarez Zarikian, M.J. Malone, and the Expedition 303/306 Scientists.North Atlantic Climate, Expeditions 303 and 306 of the riserless drilling platform from St. John's, Newfoundland, to Ponta Delgada, Azores (Portugal), Sites U1302–U1308, 25 September–17 November 2004 and from Ponta Delgada, Azores (Portugal) to Dublin, Ireland, Sites U1312–U1315, 2 March–26 April 2005 Integrated Ocean Drilling Program Management International, Inc. for the Integrated Ocean Drilling Program. Available at: http://iodp.tamu.edu/publications/exp303_306/30306title.htm, 2006.

Channell, J.E.T., Hodell, D.A., Xuan, C., Mazaud, A., Stoner, J.S., 2008. Age calibrated relative paleointensity for the last 1.5 Myr at IODP Site U1308 (North Atlantic). Earth Planet. Sci. Lett. 274, 59–71.

Channell, J.E.T., Xuan, C., Hodell, D.A., 2009. Stacking paleointensity and oxygen isotope data for the last 1.5 Myrs (PISO-1500). Earth Planet. Sci. Lett. 283, 14–23.

Cheng, H., Edwards, R.L., Broecker, W.S., Denton, G.H., Kong, X., Wang, Y., Zhang, R., Wang, X., 2009. Ice age terminations. Science 326, 248–252.

Clark, P.U., Pisias, N.G., Stocker, T.F., Weaver, A.J., 2002. The role of the thermohaline circulation in abrupt climate change. Nature 415, 863–869.

Clarke, G.K.C., Marshall, S.J., Hillaire-Marcel, C., Bilodeau, G., Veiga-Pires, C., 1999. A glaciological perspective on Heinrich Events. In: Webb, et al. (Ed.), Mechanisms of Millennial-Scale Global Climate Change. : Geoph. Monograph Series, 112. AGU, pp. 243–262.

Coplen, T.B., 1996. New guidelines for the reporting of stable hydrogen, carbon, and oxygen isotope ratio data. Geochim. Cosmochim. Acta 60, 3359.

Denton, G.H., Anderson, R.F., Toggweiler, J.R., Edwards, R.L., Schaefer, J.M., Putnam, A.E., 2010. The last glacial termination. Science 328, 1652–1656.

Dykoski, C.A., Edwards, R.L., Cheng, H., Yuan, D., Cai, Y., Zhang, M., Lin, Y., Qing, J., An, Z., Ravenaugh, J., 2005. A high-resolution, absolute-dated Holocene and deglacial Asian monsoon record from Dongge Cave, China. Earth Planet. Sci. Lett 233, 71–86.
Elliot, M., Labeyrie, L., Bond, G., Cortijo, E., Turon, J.L., Tisnerat, N., Duplessy, J.C., 1998. Millennial-scale iceberg discharges in the Irminger Basin during the last glacial period: relationship with the Heinrich events and environmental settings. Paleoceanography 13, 433–446.
Expedition 303 Scientists, Site U1302 and U1303. In: Channell, J.E.T., Kanamatsu, T., Sato, T., Stein, R., Alvarez Zarikian, C.A., Malone, M.J., Expedition 303/306 Scientists, Proc. IODP, 303: College Station TX (Integrated Ocean Drilling Program Management International, Inc.), doi:10.2204/iodp.proc.303306.103.2006, 2006.
Grousset, F.E., Labeyrie, L., Sinko, J.A., Cremer, M., Bond, G., Duprat, J., Cortijo, E., Huon, S., 1993. Patterns of ice-rafted detritus in the glacial North Atlantic (40-55°N). Paleoceanography 8, 175–192.
Heinrich, H., 1988. Origin and consequences of cyclic ice rafting in the northeast Atlantic Ocean during the past 130,000 years. Quat. Res. 29 (88), 90057–90059. doi:10.1016/0033-5894.
Hemming, S.R., 2004. Heinrich events: massive late Pleistocene detritus layers of the North Atlantic and their global climate imprint. Rev. Geophys. 42, RG1005. doi:10.1029/2003RG000128.
Hesse, R., Klaucke, I., Ryan, W.B.F., Piper, D.J.W., 1997. Ice-sheet sourced juxtaposed turbidite systems in Labrador Sea. Geosci. Can. 24 (1), 3–12.
Hesse, R., Rashid, H., Khodabakhsh, S., 2004. Fine-grained sediment lofting from meltwater-generated turbidity currents during Heinrich events. Geology 32, 449–452.
Hillaire-Marcel, C., 2011. Foraminifera isotopic records, with special attention to high northern latitudes and the impact of sea-ice distillation processes. Integrated Ocean Drilling Program, Summer School, IOP Conf. Series. Earth Environ. Sci. 14, 012009. doi:10.1088/1755-1315.
Hillaire-Marcel, C., Bilodeau, G., 2000. Instabilities in the Labrador Sea water mass structure during the last glacial cycle. Can. J. Earth Sci. 37, 795–809.
Hillaire-Marcel, C., de Vernal, A., 2008. Stable isotope clue to episodic sea ice formation in the glacial North Atlantic. Earth Planet. Sci. Lett. 268 (1–2), 43–150.
Hillaire-Marcel, C., de Vernal, A., Bilodeau, G., Wu, G., 1994. Isotope stratigraphy, sedimentation rates, deep circulation, and carbonate events in the Labrador Sea during the last 200 ka. Can. J. Earth Sci. 31, 63–89.
Hillaire-Marcel, C., de Vernal, A., Piper, D.J.W., 2007. Lake Agassiz final drainage event in the northwest North Atlantic. Geophys. Res. Lett. 34, L15601. doi:10.1029/2007GL030396.
Hillaire-Marcel, C., de Vernal, A., McKay, J., 2011. Foraminifer isotope study of the Pleistocene Labrador Sea, northwest North Atlantic (IODP Sites 1302/03 and 1305), with emphasis on paleoceanographical differences between its "inner" and "outer" basins. Mar. Geol 279, 188–198. doi:10.1016/j.margeo.2010.11.001.
Hiscott, R.N., Aksu, A.E., Mudie, P.J., Parsons, D.F., 2001. A 340,000 year record of ice rafting, paleoclimatic fluctuations, and shelf crossing glacial advances in the southwestern Labrador Sea. Glob. Planet. Change 28, 227–240.
Hodell, D.A., Curtis, J.H., 2008. Oxygen and carbon isotopes of detrital carbonate in North Atlantic Heinrich events. Mar. Geol. 256, 30–35.
Hodell, D.A., Channell, J.E.T., Curtis, J.H., Romero, O.E., Röhl, U., 2008. Onset of "Hudson Strait" Heinrich events in the eastern North Atlantic at the end of the middle Pleistocene transition (~640 ka)? Paleoceanography 23, PA4218. doi:10.1029/2008PA001591.
Hughes, T., 2011. A simple holistic hypothesis for the self-destruction of ice sheets. Quat. Sci. Rev. 30, 1829–1845.
Ji, J., Ge, Y., Balsam, W., Damuth, J.E., Chen, J., 2009. Rapid identification of dolomite using a Fourier Transform Infrared Spectrometer (FTIR): a fast method for identifying Heinrich events in IODP Site U1308. Mar Geol. 258, 60–68.
King, J.W., Banerjee, S.K., Marvin, J., 1983. A new rock-magnetic approach to selecting sediments for geomagnetic paleointensity studies: application to paleointensity for the last 4000 years. J. Geophys. Res. 88 (1983), 5911–5921.
Kirschvink, J.L., 1980. The least squares lines and plane analysis of paleomagnetic data. Geophys. J.R. Astr. Soc. 62, 699–718.
Kleiven, H.F., Kissel, C., Laj, C., Ninnemann, U.S., Richter, T.O., Cortijo, E., 2008. Reduced North Atlantic deep water coeval with glacial Lake Agassiz freshwater outburst. Science 319, 60–64.
Levi, S., Banerjee, S.K., 1976. On the possibility of obtaining relative paleointensities from lake sediments. Earth Planet. Sci. Lett 29, 219–226.
Lisiecki, L.E., Lisiecki, P.A., 2002. Application of dynamic programming to the correlation of paleoclimate records. Paleoceanography 17, 1049. doi:10.1029/2001PA000733.
Lisiecki, L.E., Raymo, M.E., 2005. A Pliocene–Pleistocene stack of 57 globally distributed benthic $d^{18}O$ records. Paleoceanography 20, PA1003. doi:10.1029/2004PA001071.
Lisiecki, L.E., Raymo, M.E., 2009. Diachronous benthic $\delta^{18}O$ responses during late Pleistocene terminations. Paleoceanography 24, PA3210. doi:10.1029/2009PA001732.
MacAyeal, D.R., 1993. Binge/purge oscillations of the Laurentide ice sheet as a cause of the North Atlantic Heinrich events. Paleoceanography 8, 775–784.
Marshall, S.J., Clark, P.U., 2002. Basal temperature evolution of North American ice sheets and implications for the 100-kyr cycle. Geophys. Res. Lett. 29, 2214. doi:10.1029/2002GL015192.
McManus, J.F., Oppo, D.W., Cullen, J.L., 1999@. A 0.5-million-year record of millennial-scale climate variability in the North Atlantic. Science 283, 971–975.
Naafs, B.D.A., Hefter, J., Ferretti, P., Stein, R., Haug, G.H., 2011. Sea surface temperatures did not control the first occurrence of Hudson Strait Heinrich Events during MIS 16. Paleoceanography 26, PA4201. doi:10.1029/2011PA002135.
Peck, V.L., Hall, I.R., Zahn, R., Grousset, F., Hemming, S.R., Scourse, J.D., 2007. The relationship of Heinrich events and their European precursors over the past 60 ka BP: a multi-proxy ice-rafted debris provenance study in the North East Atlantic. Quatern. Sci.Rev. 26, 862–875.
Rashid, H., Hesse, R., Piper, D.J.W., 2003. Evidence for an additional Heinrich event between H5 and H6 in the Labrador Sea. Paleoceanography 18 (4), 1077. doi:10.1029/2003PA000913.
Rasmussen, T.L., Oppo, D.W., Thomsen, E., Lehman, S.J., 2003. Deep sea records from the southeast Labrador Sea: ocean circulation changes and ice-rafting events during the last 160,000 years. Paleoceanography 18 (1), 1018. doi:10.1029/2001PA000736.
Robinson, S.G., Maslin, M.A., McCave, I.N., 1995. Magnetic susceptibility variations in Upper Pleistocene deep-sea sediments of the NE Atlantic: implications for ice rafting and paleocirculation at the last glacial maximum. Paleoceanography 10, 221–250.
Ruddiman, W.F., 1977. Late Quaternary deposition of ice-rafted sand in the subpolar North Atlantic (lat. 40 to 65 N). Geol. Soc. Am. Bull. 88, 1813–1827.
Scourse, J.D., Hall, I.R., McCave, I.N., Young, J.R., Sugdon, C., 2000. The origin of Heinrich layers: evidence from H2 for European precursor events. Earth Planet. Sci. Lett. 182, 187–195.
Scourse, J.D., Haapaniemi, A.I., Colmenero-Hidalgo, E., Peck, V.L., Hall, I.R., Austin, W.E.N., Knutz, P.C., Zahn, R., 2009. Growth, dynamics and deglaciation of the last British–Irish ice sheet: the deep-sea ice-rafted detritus record. Quaternary Science Reviews 28, 3066–3084.
Skinner, L.C., Shackleton, N.J., 2005. An Atlantic lead over Pacific deep-water change across Termination I: implications for the application of the marine isotope stage stratigraphy. Quat. Sci. Revs. 24, 571–580.
Sparks, R.S.J., Bonnecaze, R.T., Huppert, H.E., Lister, J.R., Hallworth, M.A., Mader, H., Phillips, J., 1993. Sediment-laden gravity currents with reversing buoyancy. Earth Planet. Sci Lett. 114, 243–257.
Stein, R., Hefter, J., Grutzner, J., Voelker, A., Naafs, B.D.A., 2009. Variability of surface water characteristics and Heinrich-like events in the Pleistocene mid-latitude North Atlantic Ocean: biomarker and XRD records from IODP Site U1313 (MIS 16–9). Paleoceanography 24, PA2203. doi:10.1029/2008PA001639.
Stoner, J.S., Channell, J.E.T., Hillaire-Marcel, C., 1995. Late Pleistocene relative geomagnetic paleointensity from the deep Labrador Sea: regional and global correlations. Earth Planet. Sci. Lett. 134, 237–252.
Stoner, J.S., Channell, J.E.T., Hillaire-Marcel, C., 1996. The magnetic signature of rapidly deposited detrital layers from the deep Labrador Sea: relationship to North Atlantic Heinrich layers. Paleoceanography 11, 309–325.
Stoner, J.S., Channell, J.E.T., Hillaire-Marcel, C., 1998. A 200 kyr geomagnetic chronostratigraphy for the Labrador Sea: indirect correlation of the sediment record to SPECMAP. J.S. Stoner, J.E.T. Channell and C. Hillaire-Marcel. Earth Planet. Sci. Letters 159, 165–181.
Stoner, J.S., Channell, J.E.T., Hillaire-Marcel, C., Kissel, C., 2000. Geomagnetic paleointensity and environmental record from Labrador Sea core MD95-2024: global marine sediment and ice core chronostratigraphy for the last 110 kyr. Earth Planet Sci. Letters 183, 161–177.
Tauxe, L., 1993. Sedimentary records of relative paleointensity of the geomagnetic field: theory and practice. Rev. Geophys. 31 (1993), 319–354.
Toews, M.W., Piper, D.J.W., 2002. Recurrence intervals of seismically triggered mass-transport deposits at Orphan Knoll continental margin off Newfoundland and Labrador. Curr. Res. Geol. Surv. Can. E17, 1–8.
Van Kreveld, S.A., Knappertsbusch, M., Ottens, J., Ganssen, G., van Hinte, J., 1996. Biogenic carbonate and ice-rafted debris (Heinrich layer) accumulation in deep-sea sediments from a Northeast Atlantic piston core. Mar. Geol. 131, 21–46.
Veiga-Pires, C., Hillaire-Marcel, C., 1998. U–Th isotope constraints on the duration of Heinrich events H0 to H4 in the southeastern Labrador Sea. Paleoceanography 14, 187–199.
Venz, K.A., Hodell, D.A., Stanton, C., Warnke, D.A., 1999. A 1.0 myr record of glacial North Atlantic intermediate water variability from ODP Site 982 in the northeast Atlantic. Paleoceanography 14, 42–52.
Walden, J., Wadsworth, E., Austin, W.E.N., Peters, C., Scourse, J.D., Hall, I.R., 2006. Compositional variability of ice-rafted debris in Heinrich layers 1 and 2 on the northwest European continental slope identified by environmental magnetic analyses. J. Quaternary Sci. 22, 163–172.
Wang, Y.J., Cheng, H., Edwards, R.L., An, Z.S., Wu, J.Y., Shen, C.-C., Dorale, J.A., 2001. A high-resolution absolute-dated Late Pleistocene monsoon record from Hulu Cave, China. Science 294, 2345–2348.
Wang, Y., Cheng, H., Edwards, R.L., Kong, X., Shao, X., Chen, S., Wu, J., Jiang, X., Wang, X., An, Z., 2008. Millennial- and orbital-scale changes in the East Asian monsoon over the past 224,000 years. Nature 451, 1090–1093.
Weeks, R., Laj, C., Endignoux, L., Fuller, M., Roberts, A., Manganne, R., Blanchard, E., Goree, W., 1993. Improvements in long-core measurement techniques: applications in palaeomagnetism and palaeoceanography. Geophys. J. Int. 114, 651–662.
Xuan, C., Channell, J.E.T., 2009. UPmag: MATLAB software for viewing and processing u-channel or other pass-through paleomagnetic data. Geochem. Geophys. Geosyst. 10, Q10Y07. doi:10.1029/2009GC002584.